

# Supplementary Materials for

## **Water-based UV-ozone activation enables aggregation-free processing of MFI nanosheets for membrane fabrication**

Pingping Li *et al.*

\* Corresponding author email: kemalcelebi@intl.zju.edu.cn

### **This PDF file includes:**

Figs. S1 to S7

Tables S1 to S4

**Fig. S1.**

**$^1\text{H}$  NMR (400 MHz, DMSO- $d_6$ ) of dC5.**  $\delta$  3.24 – 3.12 (m, 16H), 1.65 (dq,  $J = 19.9, 8.4, 7.1$  Hz, 16H), 1.29 (p,  $J = 7.4$  Hz, 2H), 0.91 (t,  $J = 7.2$  Hz, 18H).

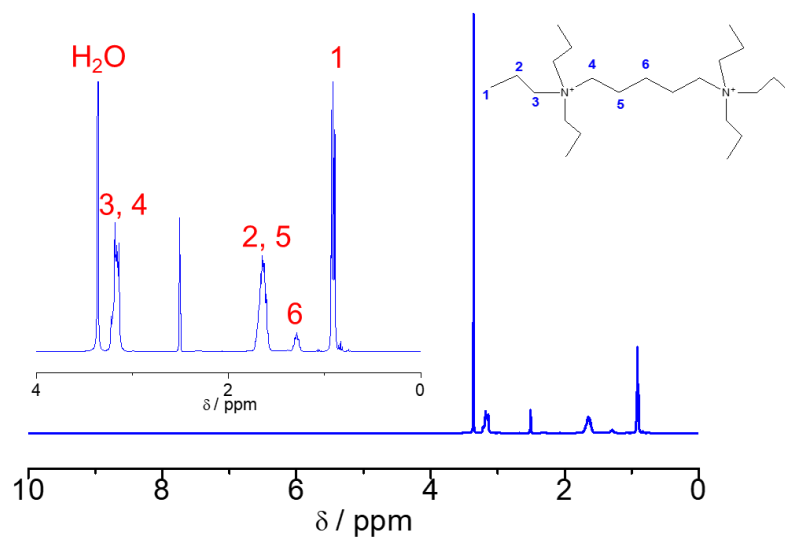


**Fig. S2.**

**Pore size distribution for the NSs obtained from various strategies.** The pore size distribution for the nanosheets obtained using piranha treatment and as-synthesized nanosheets is not shown in this study due to their low surface area. Both materials exhibited minimal microporosity, which was not detectable using the standard characterization methods employed. As a result, the pore distribution for these samples could not be accurately measured, and therefore, was not included in the data presented.

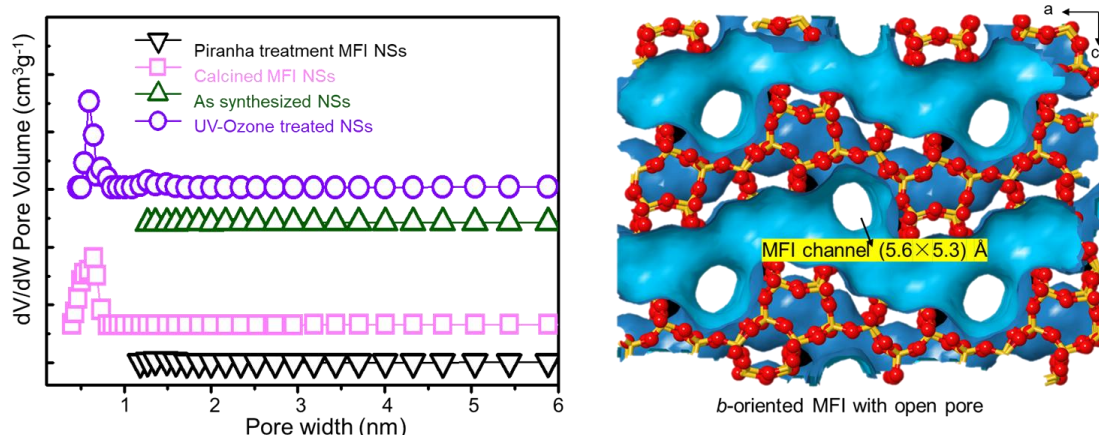


**Fig. S3.**

**Comparison of nitrogen content in as-synthesized and UV-treated nanosheets via SEM-EDX.**

**a-e**, Elemental analysis of UV-treated nanosheets, showing a residual nitrogen content of 0.15–0.27%, which is attributed to the adsorption of atmospheric nitrogen in the open-pore structure. **f**, Corresponding EDX spectrum. **g-k**, Elemental analysis of as-synthesized nanosheets, revealing a nitrogen content of 0.8–1.23%, primarily due to the presence of template agents. **l**, Corresponding EDX spectrum.

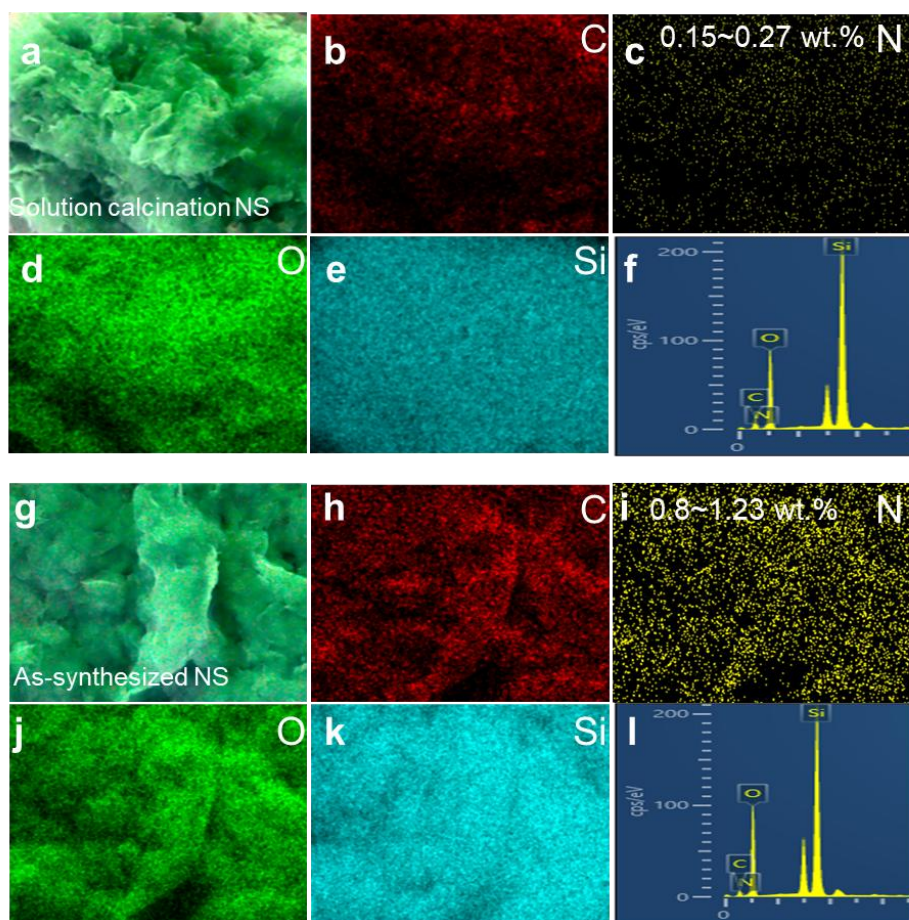


**Fig. S4.**

**UV treatment process for template removal from nanosheets.** **a**, Initial state of the nanosheets dispersed in an aqueous solution, appearing milky white. **b**, The reaction vessel wrapped in aluminum foil, where significant bubble formation is observed at the top of the solution after 12-36 hours of UV irradiation. **c**, The solution after 72 hours of UV irradiation, appears clear and transparent, indicating the complete removal of the template agents.

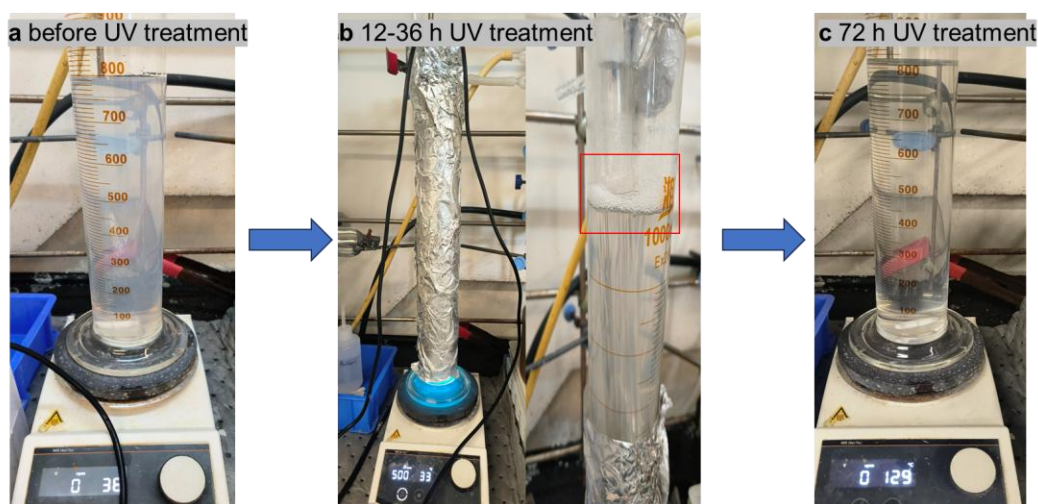


**Fig. S5.**

**Effect of high loading on the morphology of MMMs. a-b,** SEM top-view images of MMMs with a loading exceeding 10 wt.%. **c-d,** Cross-sectional images showing the formation of cavities due to increased loading.

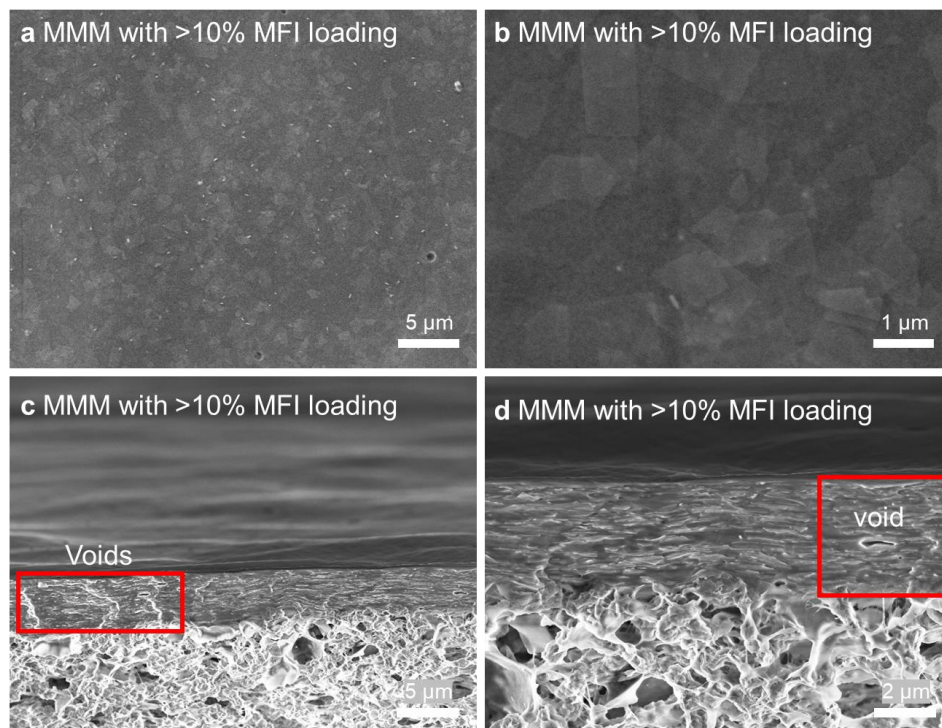


**Fig. S6.**

**Schematic illustration of the gas permeation test setup using a four-port membrane cell.** The orange layer represents the MFI-based MMM, assembled in the cell with (i) a rubber O-ring as the sealing layer, (ii) the MMM as the selective layer, and (iii) a stainless-steel disk as the support to prevent membrane crack under high pressure. An equimolar mixture of CO<sub>2</sub> and N<sub>2</sub> is introduced from the upper inlet of the cell, flows across the membrane surface, and permeates through the membrane. The permeate stream is swept by He from the lower left port and carried to the GC for compositional analysis. The right-side port of the cell is connected to the GC for detecting the feed-side composition, while the upper right port serves as the retentate outlet, where the non-permeated gas exits the system.

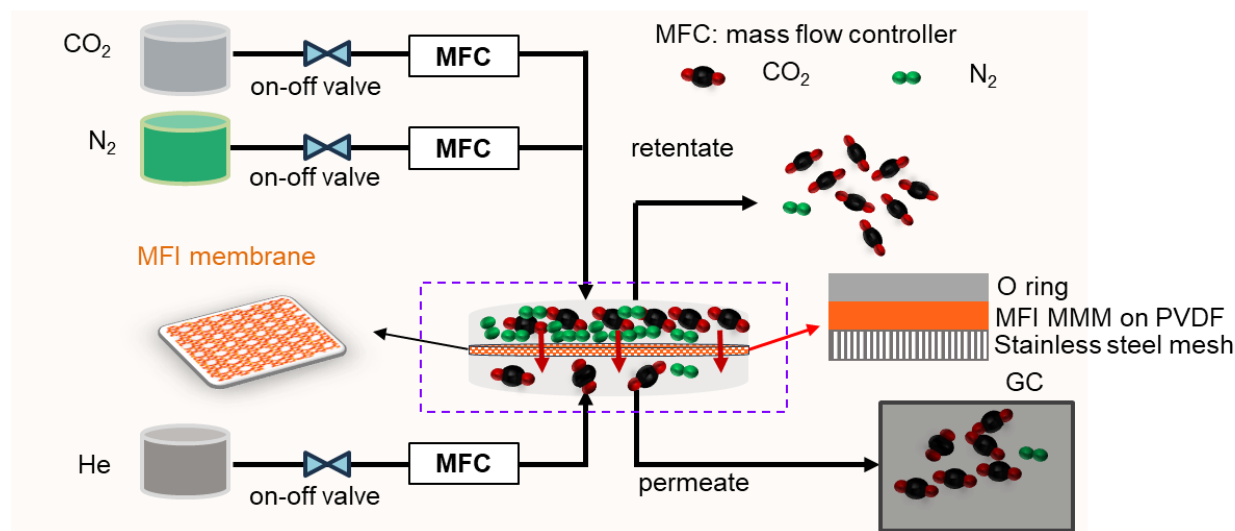




**Fig. S7.**

**CO<sub>2</sub> permeability (Barrer) in Figure 6a is derived by multiplying the measured flux ( $3.35 \times 10^{-10} \text{ mol}/(\text{m}^2 \cdot \text{s} \cdot \text{Pa})$ ) by membrane thickness.** The result demonstrates that calculated permeability increases with thickness due to the nature of the unit conversion.

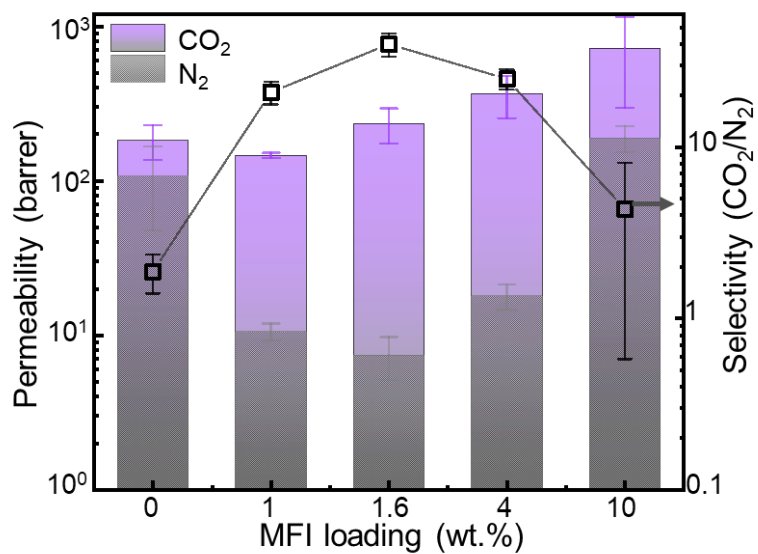




**Table S1. TGA analysis for as-synthesized NS, UV-treated NS, piranha-treated NS, and calcined NS.**

sample	Weight loss (%) at 130°C	Weight loss (%) at 500°C	Weight loss (%) at 600°C	dC5 remain (%)&
as-synthesized	1.5	16.2	17.1 <sup>*</sup>	15.6 (refer to 100%)
calcined	6.6	7.4	7.5 <sup>#</sup>	0.9 (refer to 0%)
Piranha-treated NS	2.2	15	15.6	13.4
UV-treated NS	6.2	8	10.6	4.4 (include silanol)

\* Refer to 100% dC5 remain

# Refer to 0% dC5 remain

& The remaining dC5 (%) was calculated as the weight loss at 600°C minus the weight loss at 130°C.










**Table S2. A summary of the separation performance of PVDF-supported thin *b*-oriented MFI MMMs with different loadings for CO<sub>2</sub>/N<sub>2</sub> separation at room temperature and 1 bar.**
















<b>MFI loading</b>	<b>Permeance of CO<sub>2</sub> (GPU)</b>	<b>Selectivity of CO<sub>2</sub>/N<sub>2</sub></b>
Bare PVDF	2977±41	1±0
0%	365±93	2±1
0.8%	145±6	21±3
1.6%	194±50	40±6
4%	182±55	25±3
10%	126±85	4±3











**Table S3. A summary of the separation performance of MMMs with 1.6% loading for CO<sub>2</sub>/N<sub>2</sub> separation at room temperature and 1 bar.**

<b>MFI</b>	<b>Permeance of</b>	<b>Selectivity of</b>
<b>MMM</b>	<b>CO<sub>2</sub> (GPU)</b>	<b>CO<sub>2</sub>/N<sub>2</sub></b>
M1	199±6	47±4
M2	153±4	33±1
M3	162±10	43±6
M4	263±8	36±4
Average	194±7	40±4

**Table S4. Summary of CO<sub>2</sub>/N<sub>2</sub> separation performance of zeolite MMMs from literature (shown in Fig. 5f) for comparison.**

MMM	Thickness ( $\mu\text{m}$ )	Permeance of CO <sub>2</sub> (GPU)	selectivity	Symbol	ref
MCM-48	/	0.1	16.43		49
Mg-MCM-41	100	10.2	23		50
MCM-41	60	0.17	32		56
CHA (SSZ-39)	100	189	43.2		37
CHA (SSZ-39)	100	83.1	59		37
CHA (SAPO-34)	70	0.41	58.6		52
CHA (SAPO-34)	70	0.11	26.3		53
CHA (SAPO-34)	70	4.49	26.1		55
CHA (SAPO-34)	2	40.95	22.3		64

CHA (SAPO-34)	1	2.2	10.5		65
Zeolite A-3 (nanocrystals)	/	1	20		48
4A	40	0.05	31.5		60
4A	30	0.01	102		62
NiY	50	0.04	39		59
NaY	50	14.8	57		59
NaY	30	0.2	27		61
Nano-size MFI	200	12	28.8		44
ZSM-5 (MFI)	150-250	0.01	6.6		45
ZSM-5(MFI)	150-250	0.01	3		45
ZSM-5 (MFI)	/	3	20.6		46
ZSM-5(MFI)	100	1.14	22.5		47
Silicalite (MFI)	100	7	25		50
MFI	90	0.1	21		51
ZSM-5(MFI)	70.6	1	20		54

Silicalite	70	0.14	26.3		55
(MFI)					
Pillared MFI	50-80	5	1.15		57
NSs					
ZSM-5(MFI)	50	0.29	47.1		58
ZSM-5 (MFI)	20	2	52.2		63
platelike MFI	5	37	16.7		14
platelike MFI	11.8	8.91	18.18		14
		250.23	31.94		
		147.52	18.96		
This work		145.40	20.92		
(MFI NSs)		262.92	36.44		
		177.19	26.30	